Letter

Disorder in cellular packing can alter proliferation dynamics to regulate growth

Chandrashekar Kuyyamudi,[1,2] Shakti N. Menon,[1] Fernando Casares,[3] and Sitabhra Sinha[1,2]
[1]*The Institute of Mathematical Sciences, CIT Campus, Taramani, Chennai 600113, India*
[2]*Homi Bhabha National Institute, Anushaktinagar, Mumbai 400094, India*
[3]*CABD, CSIC-Universidad Pablo de Olavide-JA, 41013 Seville, Spain*

(Received 13 July 2021; accepted 8 November 2021; published 19 November 2021)

The mechanisms by which an organ regulates its growth are not yet fully understood, especially when the cells are closely packed as in epithelial tissues. We explain growth arrest as a collective dynamical transition in coupled oscillators on disordered lattices. As the cellular morphologies become homogeneous over the course of development, the signals induced by cell-cell contact increase beyond a critical value that triggers coordinated cessation of the cell-cycle oscillators driving cell division. Thus, control of cell proliferation is causally related to the geometry of cellular packing.

DOI: 10.1103/PhysRevE.104.L052401

A central question in biology is how do individual organs, or indeed an entire organism, know that they have attained their appropriate size and hence stop growing [1–3]. As tissues and organs are composed of large numbers of cells, each implementing intrinsic programs to regulate their division, self-organized coordination across the system [4–8] is required to arrest growth [9]. Failure to achieve this can not only result in potentially fatal deformities during development [Fig. 1(a)] but can also lead to cancer later in the adult stage through unchecked growth [10,11]. As growth is primarily due to cell proliferation via mitotic division [2], the key to ensuring the appropriate final size for any developing system lies in controlling the cell cycle which regulates mitosis. As transitions between different stages of the cell cycle are governed by oscillations in the concentrations of cyclin proteins [12,13], preventing further cell division once the system has reached optimal size requires a mechanism for ensuring coordinated cessation of these intracellular oscillations. While it is known that increasing cell density can eventually arrest growth via contact inhibition of proliferation (CIP) [14–19] [see Fig. 1(b)], in general the processes through which signals encoding intercellular contact events modulate the oscillatory dynamics are not fully understood.

Terminating growth at the appropriate time is particularly challenging in tissues comprising epithelial cells, which are present in most organs of the body [2]. As adjacent cells remain in contact during growth of epithelial sheets over the course of development, contact inhibition cannot be invoked to explain the arrest of growth [20]. Understanding the process that stops further cell division in such systems is important, as uncontrolled proliferation in epithelia is linked to more than 85% of all human cancers [21,22]. While it is generally believed that the Hippo intracellular signaling pathway [16,23–29] plays a crucial role in transducing increased mechanical tension among cells that result from growth in order to inhibit proliferation [30], the mechanism linking these is yet to be fully understood. As the morphological characteristics of cells (e.g., size and shape) continually change in a growing epithelial sheet, an intriguing possibility is that the local geometry of cell-cell interfaces convey information about the state of the growing organ to the intracellular signaling pathway which can eventually arrest the cell-cycle oscillations. More generally, regulation of growth could be viewed as an emergent feature of the collective dynamics in a disordered lattice of coupled oscillators with a dynamically evolving contact geometry.

In this Letter, we propose a unified framework that describes both CIP resulting from the increase in cellular contacts with rising density, as well as growth termination triggered by morphological changes in confluent epithelial sheets. We show both to be consequences of arresting the cell-cycle oscillator by a signal whose intensity conveys information about the geometry of intercellular interfaces. As the heterogeneity of cellular morphological characteristics decreases over the normal course of development, implemented here by generating progressively more homogeneous packings in lieu of incorporating explicit cell division, it triggers a coordinated cessation of oscillations across the system. This suggests that arrest of growth can arise exclusively through changes in local cell-cell contact geometry as the organ size increases. Expressing the oscillator frequency as a function of the signal intensity and its coupling with the oscillator, we show that beyond a critical coupling strength, the system exhibits a transition to oscillation arrest as the signal intensity increases. Indeed, the strength of coupling defines two contrasting regimes characterized by opposing responses of the growth rate to increasing heterogeneity, a result that has intriguing implications for pathologies such as developmental dysplasia and cancer. Earlier models (see, e.g., Refs. [31–35]) proposed to explain growth regulation have mostly focused on mechanical feedback associated with cell growth and division and/or dynamic changes in growth-promoting signals. While our proposed mechanism can work in conjunction with these other proposed mechanisms (e.g., mechanical feedback

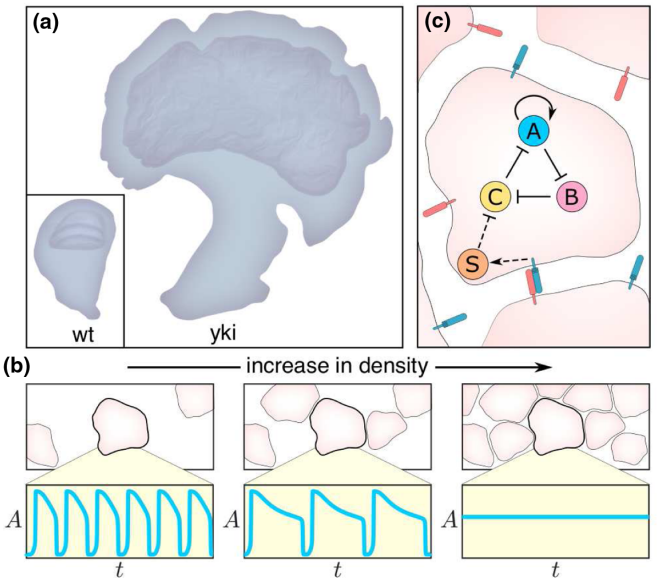

FIG. 1. Increased contact with neighbors over time results in a decreasing rate of cell division, culminating in growth arrest. (a) Schematic diagram showing an overgrown *Drosophila* imaginal disk (compared to the wild type, wt, shown in the inset) resulting from the overexpression of *yorkie* (yki), the main transcriptional effector of the Hippo signaling pathway (figure adapted from Ref. [24]). (b) The time-varying concentration A of a representative molecular species constituting the oscillator of a cell is shown at three instances in which it has progressively more surface in contact with adjacent cells. The frequency of the oscillations (governing the rate of cell division) decreases as the total contact area increases, eventually culminating in oscillator death and termination of cell division. (c) Proposed mechanism for the regulation of cell-cycle oscillations by contact-mediated signaling. A receptor (blue) binding to a ligand (orange) from a neighboring cell triggers a signaling cascade whose terminal effector molecule S regulates the cell-cycle oscillator, represented by the loop comprising molecules A, B, and C.

resulting in local variations in the intercellular interaction strengths, which is one of the key parameters in our proposed mechanism), we would like to stress that, independent of any other mechanisms, the change in the disorder of the cellular packing by altering the interface geometry can control growth rate so as to bring about the observed regulation of tissue growth giving rise to their characteristic shape and size.

To explore how self-organized arrest of tissue growth can arise over the course of development, we investigate a model of a two-dimensional (2D) sheet of cells, in which the cell-cycle oscillations governing proliferation, and hence tissue growth, are regulated by contact-mediated signaling [Fig. 1(c)]. Receptors on the surface of a cell can bind to membrane-bound ligands of a neighboring cell in close physical proximity, eventually triggering a signaling cascade (such as the Hippo pathway). This is coupled to the cell-cycle oscillator by assuming that a downstream effector molecule of the cascade, whose magnitude S conveys information about the local extracellular ligand concentration, represses one of the molecular components of the oscillator. For concreteness, we use an oscillator involving three molecular species (one of which is self-activating) that repress each other in a cyclic manner [Fig. 1(c)]. It is capable of oscillating with an almost invariant amplitude over a wide range of frequencies [36], a desirable property as cell division rates can vary widely within the same organism. Expressing the concentrations of the activated forms of the molecules as A, B, and C, the dynamics of the system upon coupling to S (via C [37]) can be described by the following set of equations:

$$\frac{dA}{dt} = \left[k_1 + \frac{k_7 A^h}{K^h + A^h}\right](A_T - A) - \frac{k_2 C^h}{K^h + C^h}A\,, \quad (1)$$

$$\frac{dB}{dt} = k_3(B_T - B) - \frac{k_4 A^h}{K^h + A^h}B\,, \quad (2)$$

$$\frac{dC}{dt} = k_5(C_T - C) - \frac{k_6 B^h}{K^h + B^h}C - \frac{k_8 S^g}{\Psi^g + S^g}C\,, \quad (3)$$

where A_T, B_T, C_T correspond to the time-invariant total concentration of the three molecular species, respectively [38]. Each equation includes a term representing the production (involving conversion of the inactivated form of a molecular species to its activated form, and including a self-catalysis term for A) and another corresponding to inactivation (occurring through a complex formed by the activated form with its repressor via a cooperative mechanism). The inactivation of each molecular species by its repressor is modeled by a Hill function, parametrized by h and K. A similar Hill function, with parameters g and Ψ, describes the inactivation of C by S. The parameters $k_1, \ldots, k_8$ represent rate constants, with k_1, k_3, k_5, and k_7 governing the activation transitions, while k_2, k_4, and k_6 regulate the inactivation processes mediated by the corresponding repressors. The rate k_8 quantifies the coupling strength between the contact-induced signal S and the cell-cycle oscillator via the repression of C.

The cell-cycle model can be made analytically tractable by replacing the Hill functions involving A, B, C with their limiting forms, viz., Heaviside step functions: $\Theta(z) = 1$ if $z \geqslant 0$, and 0 otherwise [39]. The dynamics of this *reduced model* can be represented as trajectories between a set of discrete states represented by binary strings of length 3. The three bits indicate whether A, B, or C exceed the threshold K $(= 1)$ or not $(= 0)$ [Fig. 2(a)]. Two different attractors are observed depending on the coupling strength k_8 between the cell-cycle oscillator and the signal S. Despite the differences in the pattern of oscillations exhibited by the cell-cycle model [Eqs. (1)–(3)] and its reduced version [compare the two panels of Fig. 2(b)], the curve $k_8^*(S)$ separating the domain of these two attractors in the (k_8, S) parameter space are qualitatively similar [compare the left and central panels of Fig. 2(c)]. For the reduced model, we can derive an exact expression for $k_8^* = k_5[(C_T/K) - 1]/[S^g/(\psi^g + S^g])$, such that for $k_8 < k_8^*$, the system cycles between six states, while for $k_8 > k_8^*$, the dynamics converges to a fixed point. In the former case, the oscillation period is the sum of the time intervals spent in each state comprising the cyclic attractor. The frequency of oscillations thus obtained accurately reproduces the results of the reduced model [compare the central and right panels of Fig. 2(c)].

We note that the period of the cell cycle increases with the magnitude S of the contact-induced signal, and for large values of the coupling k_8, results in arrest of the oscillations. To reproduce a CIP-like scenario with increasing cell density

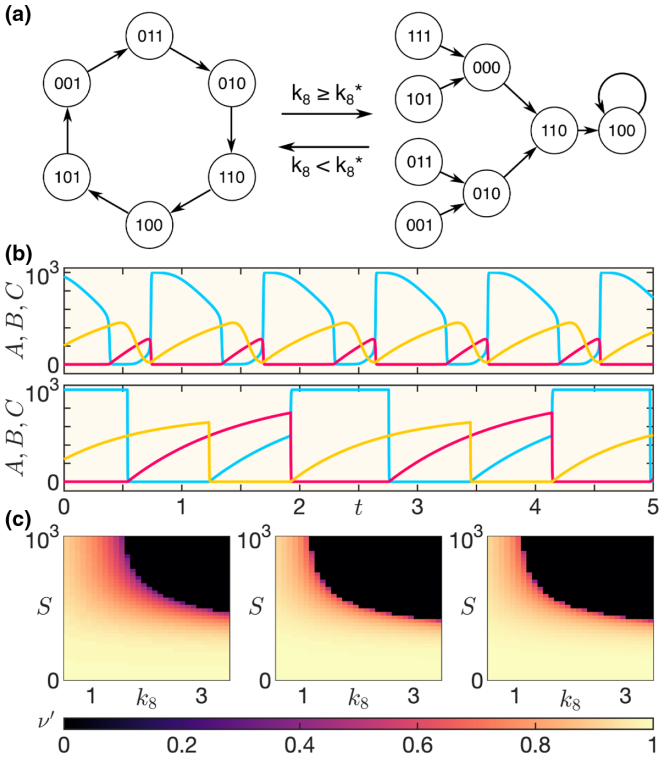

FIG. 2. Coupling-mediated dynamical transition from cell-cycle oscillations to growth arrest. (a) State transition graphs representing (left) the cyclic cellular dynamics corresponding to cell division and (right) convergence to a globally attracting steady state (100) representing a cell that has stopped dividing. The cellular states, shown as circles, are identified by binary strings whose entries indicate if the molecular concentrations of the oscillator components, viz., A, B, and C, respectively, are above a threshold value K. The cell switches from one type of dynamics to the other when the bifurcation parameter k_8, the strength of coupling between the contact-induced signal and the cell-cycle oscillator, is increased above the critical value k_8^*. (b) Comparison of the oscillations exhibited by the cell-cycle model (top) and those in the reduced model (bottom) obtained by replacing the continuous functions describing the interactions between A, B, and C with step functions. (c) The scaled oscillation frequency ν' (expressed relative to its maximum possible value) shown as a function of the magnitude of the signal S and the strength of coupling k_8. The parameter space diagram for the cell-cycle model (left) is seen to be qualitatively similar to that obtained for the reduced model (center), which in turn can be reproduced with a high degree of accuracy using a closed-form expression obtained analytically (right).

resulting from successive cell divisions, we note that the cells become more likely to come in contact with each other over time, thereby increasing S on average. This suggests that there is an effective "negative feedback" operating between the rate at which cells multiply that is governed by the oscillator, and the resultant local cell density which regulates its dynamics through contact-mediated signaling. Such a process will result in the sequence shown in Fig. 1(b), with cells initially proliferating rapidly, then slowing down over time and eventually ceasing to divide altogether as their density progressively rises. As cellular proliferation also serves to homogenize the cellular morphology in a tightly packed domain, as is the case in growing epithelial tissue [40–42], a more intriguing possibility is that changes in the sizes and shapes of cells can themselves alter the contact-induced signal. We show below that these morphological transitions can indeed control the cell-cycle periods, thereby influencing the rate at which cells proliferate.

To investigate how the rate of proliferation (controlled by the cell-cycle period) varies with the shape of the cells in a growing tissue, we consider a 2D plane tiled with nonoverlapping polygons. These are generated from Voronoi diagrams to represent the space-filling arrangement of cells in a tissue [43]. The polygons are initially obtained by randomly choosing N generating points ("seeds") uniformly distributed across the 2D domain, resulting in highly heterogeneous distributions of their areas, perimeters, and number of sides. Subsequently, Lloyd's algorithm is used to iteratively generate progressively more homogeneous arrangements of these N polygons [43]. It reproduces the evolution of the distribution of cellular geometries observed in normal development as cells proliferate (e.g., see Refs. [44,45]) without explicitly incorporating cell division into our model. This allows us to attribute the observed changes in the collective dynamics resulting in growth arrest exclusively to the altered geometry of the cellular interfaces over the course of development. We have verified that the proposed mechanism is robust in the presence of temporally increasing system size as a consequence of cell division (for details of the implementation, see Supplemental Material [39]).

The process we use to generate progressively more homogeneous cellular configurations involves replacing the seed of every Voronoi cell by an approximation of the centroid (obtained as the mean of the coordinates of many randomly generated points inside the polygon) at each iteration and recomputing the Voronoi diagram [46]. Applying this sequence of steps repeatedly results in convergence to a centroidal Voronoi tessellation (CVT) in which the centroids and generating points coincide for all cells, corresponding to the most uniform tiling of the domain with N cells. Figure 3(a) shows a representative initial arrangement of cells that are highly heterogeneous in terms of sizes and shapes (left panel). For comparison, we show alongside it the configuration (right panel) obtained after ten iterations of the algorithm described above, whose relatively higher homogeneity is visually apparent. To demonstrate this quantitatively, Fig. 3(b) shows the evolution of the distribution of the perimeters l of the N polygons tiling the plane through each step j in the transition from the initial to the final state shown in Fig. 3(a).

The homogenization of cell sizes and shapes can in turn affect the rate at which the tissue grows, as the perimeter of the cell determines the frequency of ligand-receptor binding events that trigger the signaling cascade regulating the cell cycle. Thus, we assume that the ligand concentration L_i bound to cell i is proportional to its perimeter l_i, viz., $L_i = (l_i/\langle l \rangle)L_0$, where $\langle l \rangle$ and L_0 are the average perimeter of the cells and the mean ligand concentration across the tissue, respectively. The corresponding strength of the contact-induced signal is $S_i = S_{\max} L_i^q/(K_S^q + L_i^q)$, where $S_{\max}$, K_S, and q represent the maximum signal strength, the half-saturation constant, and the Hill coefficient regulating the steepness of the response function, respectively. We have explicitly verified that other possible dependencies of the signal on cell size and shape

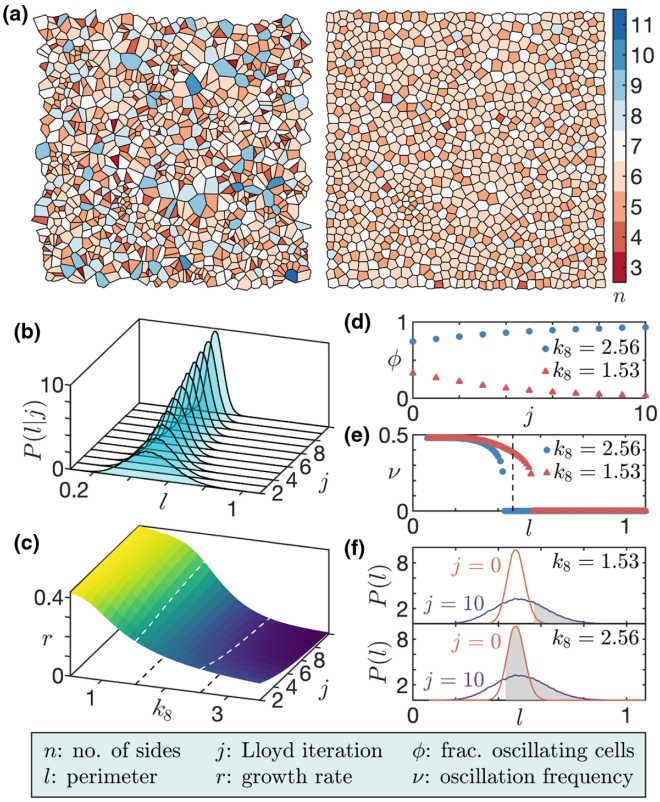

FIG. 3. Increasing homogeneity in the distribution of cell shapes can have differential outcomes depending on the coupling between the contact-induced signal and the cell-cycle oscillator. (a) Cellular packing in an epithelial sheet represented by Voronoi tessellations. The two configurations shown have the same number of cells ($N = 10^3$) but differ in the heterogeneity of the degrees k, i.e., the number of neighbors of a given cell (see colorbar). The initial heterogeneity (left) is progressively reduced using Lloyd's algorithm, as seen from the tiling shown after ten iterations (right). (b) The approach to uniformity with successive iterations j is indicated by the narrowing distribution of the cell perimeters l. (c) The tissue growth rate r, given by the mean of the frequencies of the cellular oscillators, varies with the heterogeneity (determined by the iteration j) and the bifurcation parameter k_8. Two contrasting regimes are observed as the polygons become more uniform: for higher (lower) values of k_8 the growth rate decreases (increases) as the tissue becomes more homogeneous. (d) The fraction ϕ of cells that have stopped oscillating at each iteration j and (e) the frequency of oscillations of cells having perimeter l, shown for the two regimes, viz., $k_8 = 1.53$ (triangles) and $k_8 = 2.56$ (circles) [corresponding to the dashed curves in (c)]. The broken line in (e) indicates the mean perimeter of the N cells. (f) The initial ($j = 0$, blue) and final ($j = 10$, red) distributions of l corresponding to the weak- (lower panel: $k_8 = 1.53$) and strong-coupling (upper panel: $k_8 = 2.56$) regimes. The shaded region indicates perimeters above the critical value beyond which oscillations are arrested.

(e.g., area or number of neighbors) yield results that are qualitatively similar to those reported here [39]. Figure 3(c) shows that the growth rate r of the tissue (obtained by averaging over the cell-cycle frequencies across the domain) varies systematically as the cellular configuration becomes more homogeneous (with increasing number of iterations j of the Lloyd's algorithm). However, there are two distinct regimes seen for different values of the coupling strength k_8. For stronger k_8 [$=2.56$ in Fig. 3(c)] increased homogeneity is accompanied by a slowing growth rate, while for weaker k_8 [$=1.53$ in Fig. 3(c)], r decreases with increasing heterogeneity.

To elucidate these two contrasting regimes, we first note that with increasing homogeneity, an increased fraction ϕ of cells stop oscillating when the coupling k_8 is strong, while the reverse is true for weaker k_8 [Fig. 3(d)]. This can be understood in terms of the role that the cell perimeter l, which has a monotonic relation to the magnitude of the contact-induced signal S, plays in the cell-cycle oscillator. Figure 3(e) shows that while increased l results in the oscillation frequency (and hence, the rate of cell division) decreasing eventually to 0, the critical cell size at which the oscillation is arrested is lowered as the coupling k_8 becomes stronger [consistent with Fig. 2(c)]. As increased homogeneity implies a decreasing width of the distribution of l, we can explain the differential evolution of the growth rate in the two regimes as follows. For weaker k_8, where the critical value of l is higher than the mean perimeter, we will observe a relative *increase* in the fraction of oscillating cells and also their mean frequency with decreasing width of the distribution [Fig. 3(f), upper panel]. It follows that decreasing growth rate will be associated with increasing *heterogeneity* in the weak-coupling regime. In contrast, the lower panel in Fig. 3(f) shows that for a stronger value of k_8, when the critical value of l at which oscillation is arrested is lower than the mean cellular perimeter, the fraction of oscillating cells (as well as their mean frequency) will *decrease* as the dispersion of l decreases. Thus, in this strong-coupling regime, it is increased *homogeneity* of cellular morphology that will accompany the slowing growth rate of the tissue.

To conclude, we have shown that increasing heterogeneity in cell sizes and shapes can lead to differential outcomes in the collective activity of a system of cell-cycle oscillators forming a disordered lattice, depending on the strength of the intercellular interactions that implement contact inhibition. With decreasing impact of the contact-induced signal on the cell-cycle oscillator (low k_8), we expect the growth rate to increase as the cellular arrangement becomes more irregular, as is observed in dysplasia that sometimes precedes tumor growth. Indeed, intercellular communication is known to be impeded in cancers along with an increased rate of cellular proliferation [47–49]. This can be associated in our model to a system trajectory involving both k_8 (regulating the signaling between cells) and j (controlling the disorder in cellular morphology) decreasing simultaneously, causing the proliferation rate r to increase. A possible experimental approach to verify this can involve altering the strength of cellular interactions by regulating the number of relevant cell surface receptors (e.g., by attenuating the expression of the corresponding genes) at different stages of development (corresponding to distinct regimes of disorder) and observing the subsequent change in the rate of growth of the tissue. While suppressing the components of the intercellular signaling mechanism should result in an increase in the growth rate, our results suggest that doing it at a later stage would give rise to a much higher subsequent growth rate than if the manipulation is done at a relatively early stage. Our work also suggests a causal relation between the simultaneous increase in regularity of the

planar arrangement of cells in growing epithelial tissue and the arrest of growth in the cellular assembly in normal development (i.e., strong coupling) [40,50,51]. It further suggests that heterogeneous contact topology in networks of oscillators interacting via lateral inhibition [52] will increase the range over which chimera states, characterized by the coexistence of oscillating and nonoscillating elements [53], are likely to occur.

The authors would like to acknowledge discussions during the ICTS Winter School on Quantitative Systems Biology (ICTS/qsb2019/12). S.N.M. has been supported by the Center of Excellence in Complex Systems and Data Science, funded by the Department of Atomic Energy, Government of India. The simulations required for this work were supported by IMSc High Performance Computing facility (Nandadevi).

[1] S. Gilbert, *Developmental Biology.*, 11th ed. (Sinauer, Sunderland, MA, 2018).
[2] L. Wolpert and C. Tickle, *Developmental Biology* (Oxford University Press, Oxford, 2011).
[3] M. N. Shahbazi, Development **147**, dev190629 (2020).
[4] S. De Monte, F. d'Ovidio, S. Danø, and P. G. Sørensen, Proc. Natl. Acad. Sci. USA **104**, 18377 (2007).
[5] A. F. Taylor, M. R. Tinsley, F. Wang, Z. Huang, and K. Showalter, Science **323**, 614 (2009).
[6] A. D. Lander, Science **339**, 923 (2013).
[7] M. Whiteley, S. P. Diggle, and E. P. Greenberg, Nature (London) **551**, 313 (2017).
[8] C. Kuyyamudi, S. N. Menon, and S. Sinha, Phys. Rev. E **103**, 062409 (2021).
[9] M. F. Hagan and G. M. Grason, Rev. Mod. Phys. **93**, 025008 (2021).
[10] C. J. Sherr, Science **274**, 1672 (1996).
[11] D. V. Kuznetsov and A. V. Blokhin, Phys. Rev. Lett. **85**, 2833 (2000).
[12] D. Santamaría, C. Barrière, A. Cerqueira, S. Hunt, C. Tardy, K. Newton, J. F. Cáceres, P. Dubus, M. Malumbres, and M. Barbacid, Nature (London) **448**, 811 (2007).
[13] D. A. Orlando, C. Y. Lin, A. Bernard, J. Y. Wang, J. E. Socolar, E. S. Iversen, A. J. Hartemink, and S. B. Haase, Nature (London) **453**, 944 (2008).
[14] M. Stoker and H. Rubin, Nature (London) **215**, 171 (1967).
[15] N. Šestan, S. Artavanis-Tsakonas, and P. Rakic, Science **286**, 741 (1999).
[16] B. Zhao, X. Wei, W. Li, R. S. Udan, Q. Yang, J. Kim, J. Xie, T. Ikenoue, J. Yu, L. Li *et al.*, Genes Dev. **21**, 2747 (2007).
[17] N.-G. Kim, E. Koh, X. Chen, and B. M. Gumbiner, Proc. Natl. Acad. Sci. USA **108**, 11930 (2011).
[18] A. Puliafito, L. Hufnagel, P. Neveu, S. Streichan, A. Sigal, D. K. Fygenson, and B. I. Shraiman, Proc. Natl. Acad. Sci. USA **109**, 739 (2012).
[19] K. Aoki, Y. Kumagai, A. Sakurai, N. Komatsu, Y. Fujita, C. Shionyu, and M. Matsuda, Mol. Cell **52**, 529 (2013).
[20] H. Honda, Dev. Growth Differ. **59**, 306 (2017).
[21] L. M. McCaffrey and I. G. Macara, Trends Cell Biol. **21**, 727 (2011).
[22] I. G. Macara, R. Guyer, G. Richardson, Y. Huo, and S. M. Ahmed, Curr. Biol. **24**, R815 (2014).
[23] K. F. Harvey, C. M. Pfleger, and I. K. Hariharan, Cell **114**, 457 (2003).
[24] J. Huang, S. Wu, J. Barrera, K. Matthews, and D. Pan, Cell **122**, 421 (2005).
[25] B. J. Thompson and S. M. Cohen, Cell **126**, 767 (2006).
[26] Q. Zeng and W. Hong, Cancer Cell **13**, 188 (2008).
[27] M. Kango-Singh and A. Singh, Dev. Dyn. **238**, 1627 (2009).
[28] H. Oh and K. D. Irvine, Trends Cell Biol. **20**, 410 (2010).
[29] B. M. Gumbiner and N.-G. Kim, J. Cell Sci. **127**, 709 (2014).
[30] S. Ma, Z. Meng, R. Chen, and K.-L. Guan, Annu. Rev. Biochem. **88**, 577 (2019).
[31] B. I. Shraiman, Proc. Natl. Acad. Sci. USA **102**, 3318 (2005).
[32] O. Wartlick, P. Mumcu, A. Kicheva, T. Bittig, F. Jülicher and M. Gonzalez-Gaitan, Science **331**, 1154 (2011).
[33] T. Aegerter-Wilmsen, M. B. Heimlicher, A. C. Smith, P. B. de Reuille, R. S. Smith, C. M. Aegerter and K. Basler, Development **139**, 3221 (2012).
[34] C. Gérard and A. Goldbeter, J. R. Soc. Interface **4**, 3 (2014).
[35] Y. Pan, I. Heemskerk, C. Ibar, B. I. Shraiman and K. D. Irvine, Proc. Natl. Acad. Sci. USA **113**, E6974 (2016).
[36] T. Y.-C. Tsai, Y. S. Choi, W. Ma, J. R. Pomerening, C. Tang, and J. E. Ferrell, Science **321**, 126 (2008).
[37] Qualitatively similar behavior is obtained if S is coupled to the cell-cycle oscillator via A or B (instead of C) with the only change occurring in the identity of the state to which the system converges (010 and 001, respectively, instead of 100) for $k_8 \geqslant k_8^*$.
[38] The sum of the activated and inactivated forms of the molecular species are chosen as $A_T, B_T, C_T = 1000$ each for the simulations reported here. Our results are not sensitively dependent on the exact numerical values of these parameters.
[39] See Supplemental Material at http://link.aps.org/supplemental/10.1103/PhysRevE.104.L052401 for details.
[40] M. C. Gibson, A. B. Patel, R. Nagpal, and N. Perrimon, Nature (London) **442**, 1038 (2006).
[41] T. Lecuit and L. Le Goff, Nature (London) **450**, 189 (2007).
[42] J. Devany, D. M. Sussman, T. Yamamoto, M. L. Manning, and M. L. Gardel, Proc. Natl. Acad. Sci. USA **118**, e1917853118 (2021).
[43] D. Sánchez-Gutiérrez, M. Tozluoglu, J. D. Barry, A. Pascual, Y. Mao, and L. M. Escudero, EMBO J. **35**, 77 (2016).
[44] M. Kokic, A. Iannini, G. Villa-Fombuena, F. Casares, and D. Iber, bioRxiv 590729 (2019), doi: 10.1101/590729.
[45] N. A. Dye, M. Popović, K. Venkatesan Iyer, J. F. Fuhrmann, R. Piscitello-Gómez, S. Eaton, and F. Jülicher, eLife **10**, e57964 (2021).
[46] At each step j of the algorithm, $N\,2^j$ points are chosen from a uniform distribution over the domain, which ensures an increasing spatial resolution in approximation of the centroids as the iterations proceed.
[47] K.-I. Wada, K. Itoga, T. Okano, S. Yonemura, and H. Sasaki, Development **138**, 3907 (2011).

[48] A. J. Knights, A. P. W. Funnell, M. Crossley, and R. C. M. Pearson, Trends Cancer Res. **8**, 61 (2012).
[49] Y. Yu and R. C. Elble, J. Clin. Med. **5**, 26 (2016).
[50] A.-K. Classen, K. I. Anderson, E. Marois, and S. Eaton, Dev. Cell **9**, 805 (2005).
[51] We note that the anomalous situation where the contact topology of the cells becoming more heterogeneous over time would result in higher growth rate is suggestive of the phenomenon of developmental dysplasia in which cells proliferate more rapidly in a disorderly arrangement.
[52] R. Janaki, S. N. Menon, R. Singh, and S. Sinha, Phys. Rev. E **99**, 052216 (2019).
[53] R. Singh and S. Sinha, Phys. Rev. E **87**, 012907 (2013).